Journal of Power Sources 268 (2014) 491–497

Contents lists available at ScienceDirect

Journal of Power Sources

journal homepage: www.elsevier.com/locate/jpowsour

High rate $LiMn_2O_4$/carbon nanotube composite prepared by a two-step hydrothermal process

Bang-Kun Zou [a], Xiao-Hang Ma [a], Zhong-Feng Tang [a], Chu-Xiong Ding [a], Zhao-Yin Wen [b], Chun-Hua Chen [a, *]

[a] CAS Key Laboratory of Materials for Energy Conversions, Department of Materials Science and Engineering & Collaborative Innovation Center of Suzhou Nano Science and Technology, University of Science and Technology of China, Hefei 230026, Anhui, China
[b] Shanghai Institute of Ceramics, Chinese Academy of Sciences, Shanghai 200050, China

HIGHLIGHTS

- A nanoplate-assembled MnO_2 with a high surface area is synthesized.
- The two-step hydrothermally synthesized $LiMn_2O_4$/carbon nanotube composite keeps the particle size of MnO_2 precursor.
- $LiMn_2O_4$/carbon nanotube composite shows a high rate capability and reversible cycling performance.

ARTICLE INFO

Article history:
Received 18 April 2014
Received in revised form
10 June 2014
Accepted 17 June 2014
Available online 24 June 2014

Keywords:
Lithium manganese oxide
Spinel
Carbon nanotube
Hydrothermal
Rate capability

ABSTRACT

A two-step hydrothermal approach is employed to synthesize $LiMn_2O_4$/carbon nanotube (LMO/CNT) composite powders. X-ray diffraction, scanning electron microscopy, thermal gravimetry and N_2-adsorption/desorption are used to characterize their structures and compositions. Galvanostatic cycling in coin-cells is adopted to measure their electrochemical properties as cathode materials of lithium-ion batteries. A $LiMn_2O_4$ pure phase of high crystallinity is observed with CNT homogeneously dispersed in the composite network. The electrochemical properties of them are associated with two factors, i.e. the content of CNT in the hydrothermal process and the annealing temperature at the subsequent heat treatment step. Excellent rate capability of these LMO/CNT electrodes can be achieved.

1. Introduction

Li-ion batteries (LIBs) are playing more and more important roles in our daily life as power sources for various electronic appliances and electric vehicles [1–3]. The emerging applications in large-scale energy storage systems necessitate more demanding criteria for practical LIBs, including low cost, high rate capability, improved safety and reliability [4,5]. Currently, $LiCoO_2$ and $LiFePO_4$ as two representative cathode materials are being widely used in LIBs. However, the high cost and nocuous shortcoming of $LiCoO_2$ [6–8] and the poor electronic conductivity of $LiFePO_4$ [9,10] have driven researchers to develop new cathode materials. Owing to its low cost, high potential (4 V vs. Li^+/Li), nontoxicity and fairly high electrical conductivity, the spinel-type $LiMn_2O_4$ (LMO) can overcome the shortcomings of $LiCoO_2$ and $LiFePO_4$ [11,12]. It is usually synthesized by using a manganese oxide (MnO, Mn_2O_3 or MnO_2) and a lithium salt as the precursors and sintering at high temperatures (usually above 600 °C) to obtain various microstructures [13,14], such as nanorods [15], yolk microspheres [16], hollow spheres [17,18] and solid nanoparticles [19]. On the other hand, cationic doping with some metal ions (e.g. Al^{3+}, Co^{3+} and Ni^{2+}) can improve the stability of the structure by restraining Jahn–Teller effect to have a long cycle life [20–23].

Recently, $LiMn_2O_4$/carbon composites with high power capability have been reported [24–27]. Because $LiMn_2O_4$ is typically synthesized in air in the temperature range of 600–800 °C, which is higher than the oxidation temperature of carbon (400–600 °C), such LMO/C composites cannot be obtained under these conditions. Hence a hydrothermal process is likely one of few methods to synthesize $LiMn_2O_4$/carbon composites at a low temperature. For

* Corresponding author. Tel.: +86 551 63606971; fax: +86 551 63601592.
E-mail address: cchchen@ustc.edu.cn (C.-H. Chen).

http://dx.doi.org/10.1016/j.jpowsour.2014.06.085
0378-7753/

example, carbon nanotube (CNT) is mixed with a mixed solution of $KMnO_4$ and a lithium precursor (e.g. LiOH) to obtain a suspension, which is treated hydrothermally to prepare a $LiMn_2O_4$/CNT composite powder [24–26]. However, this synthetic approach tends to have severe $LiMn_2O_4$ agglomerations, which is not beneficial for the electrochemical properties.

In this study, we develop an improved hydrothermal process by adopting a two- step approach and successfully synthesize $LiMn_2O_4$/CNT composite powders with a narrow particle distribution in the range of 700–900 nm. As a cathode material for LIBs, these $LiMn_2O_4$/CNT composites exhibit an excellent high rate capability and cycling stability.

2. Experimental

2.1. Synthesis of nanoplate-assembled MnO_2 spheres

Manganese sulphate ($MnSO_4 \cdot H_2O$, 0.51 g) was dissolved in 100 mL deionized water and stirred for 10 min to obtain a transparent solution. Then ammonium peroxydisulfate ($(NH_4)_2S_2O_8$, 1.71 g) was dissolved in the solution under vigorous stirring for 30 min. Subsequently, the solution was maintained at 70 °C for 4 h in a water bath. As a result, a precipitate of MnO_2 was produced, which was centrifuged and washed for several times with distilled water and absolute alcohol. The MnO_2 precipitate was then dried at 70 °C for 12 h in a vacuum oven.

2.2. Synthesis of $LiMn_2O_4$/CNT (LMO/CNT)

A CNT (Boyu Gaoke, Beijing) was treated in a mixed acid solution (18.4 M H_2SO_4 and 15.3 M HNO_3 in a volume ratio of 3:1) at 60 °C for 6 h. Then 0.3375 g MnO_2, which was synthesized in the above precipitation step, was mixed with 0.1125 g treated CNT (or 25 wt% CNT) and 60 mL LiOH solution (0.1 M) in a glass beaker to obtain a suspension. This suspension was ultrasonically vibrated for 30 min and stirred for 1 h. Finally, the suspension was transferred into a 100 mL Telfon-lined stainless steel autoclave and sealed. The autoclave was put into an electric oven and kept at 180 °C for 48 h. After this hydrothermal treatment, an LMO/CNT powder (S1) was collected by centrifuging and washing the resulted suspension for several times with deionized water and absolute alcohol. This LMO/CNT sample (S1) was dried at 70 °C for 12 h for further characterization. For comparison, two reference samples (S2 and S3) with less amount of CNT (20 wt% for S2 and 15 wt% for S3) were prepared by following the same procedure as described above. Also, the sample S1 was also annealed in air at 450 °C and 700 °C for 4 h, respectively, to obtain two other samples S4 and S5 which contained different amounts of carbon due to the high temperature annealing.

2.3. Morphology and structure characterization

The phase and crystallinity of the samples were characterized using powder X-ray diffraction (XRD, Rigaku) with Cu Kα radiation over a range of 2θ angles from 10° to 70°. A scanning electron microscopy (SEM, JSM-6390 LA, JEOL) study of the powders was performed to analyze their morphologies. The specific surface area and the pore size distribution were measured by N_2-adsorption/desorption (Tristar II 3020M, Micromeritics). Thermogravimetry (TGA Q5000IR) measurement was also conducted in air at a heating rate of 10 °C min^{-1} to investigate the content of the CNT in the LMO/CNT composites.

2.4. Electrochemical measurements

To evaluate the electrochemical performance of the LMO/CNT composites, CR2032-type coin-cells were assembled in an argon filled glove box (MBraun Labmaster 130) with LMO/CNT working electrodes, a lithium foil counter electrode, and a porous membrane separator (Celgard 3501). The working electrodes of the LMO/CNT S1, S2, and S3 were prepared by coating slurries of the composite powders (90 wt%) and polyvinylidene fluoride binder (10 wt%) dispersed in *N*-methyl-2-pyrrolidone onto an aluminum foil. They were then dried in vacuum oven at 120 °C for 12 h, and then roll pressed to a thickness of about 23 μm. The loading density of LMO was about 2.0 mg cm^{-2}. The electrolyte was composed of 1 M $LiPF_6$ solution in ethylene carbonate (EC) and dimethyl carbonate (DMC) (1:1, v/v, Zhuhai Smoothway Electronics Materials Co. Ltd). The cyclic voltammetry (CV) and electrochemical impedance spectroscopy (EIS) of the cells were conducted on a CHI 604A electrochemical workstation. The CV was measured in a voltage range from 3.0 to 4.5 V at a scan rate of 0.1 mV s^{-1}. The cells were also galvanostatically cycled on a multi-channel battery test system (Neware BTS-2300, Shenzhen) in the voltage range from 3.0 to 4.5 V.

3. Results and discussion

Fig. 1 illustrates the XRD patterns of the MnO_2, CNT, LMO/CNT or LMO samples synthesized under different conditions. It can be seen that the MnO_2 powder obtained from the oxidation of manganese sulphate exhibits a pure ramsdellite phase with lower crystallinity (pattern a). The acidification treated CNT gives a typical diffraction pattern of carbon nanotube with a characteristic peak at 26.4° (pattern b). After the hydrothermal step, the obtained samples S1–S3 demonstrate diffraction peaks which can be indexed into a well-crystalline spinel-type $LiMn_2O_4$ phase and a CNT (patterns c–e). After the annealing of LMO/CNT at 450 °C or 700 °C in air, only the diffraction peaks of LMO can be detected (patterns f, g), indicating that at least most of CNT component has been burned out.

Fig. 2 shows the results of the SEM and N_2-adsorption/desorption analyses of the intermediate product MnO_2. It can be clearly seen that the MnO_2 powder is composed of burr-like spheres with a uniform particle size of about 800 nm (Fig. 2a). Each sphere is porous and constituted with many nanoplates (Fig. 2b). A self-assembly mechanism must have occurred during the redox process in a water bath. The N_2-sorption analysis gives a type-IV isotherm (Fig. 2c), which results in a pore size distribution between 5 and 10 nm (Fig. 2d). Therefore, the MnO_2 sample is a

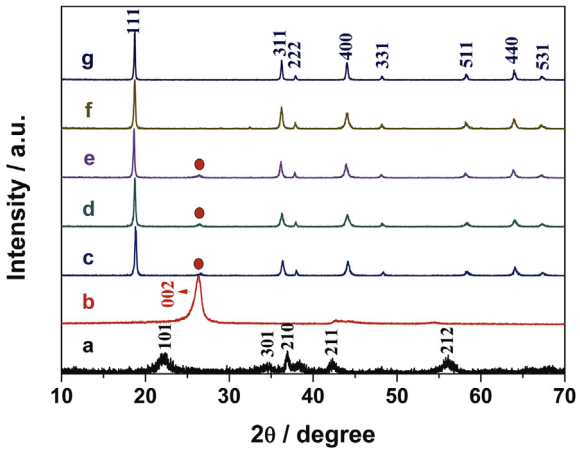

Fig. 1. XRD patterns of MnO_2 (a), acidification treated CNT (b), LMO/CNT with different amount of CNT (c–e): 15 wt% (S3), 20wt% (S2) and 25 wt% (S1), and S4 (f) and S5 (g) which were obtained by annealing S1 at 450 °C and 700 °C for 4 h in air.

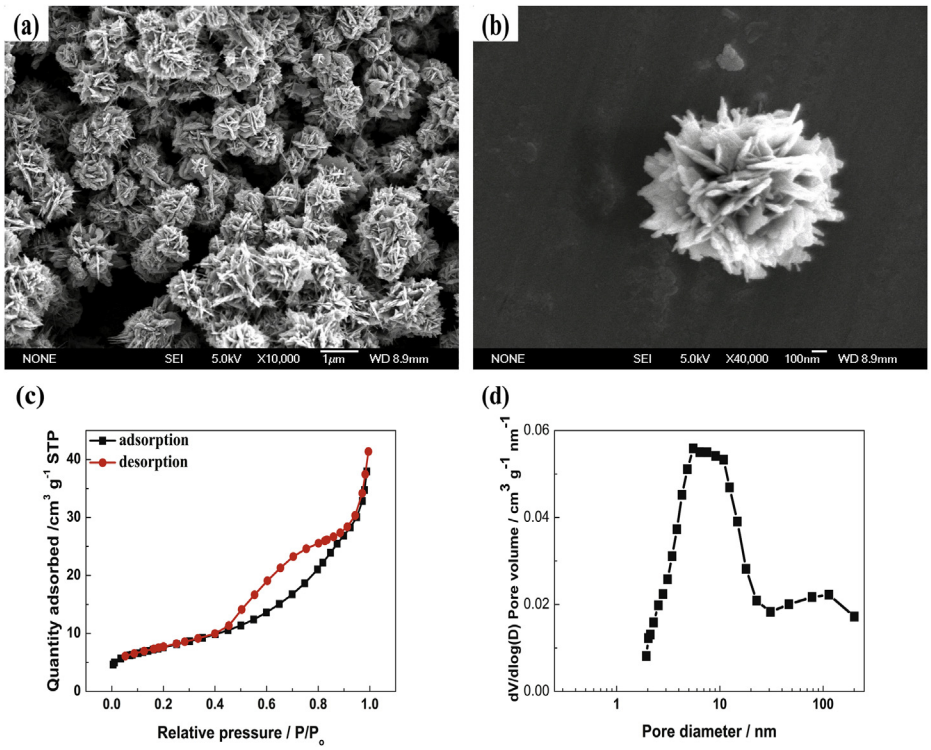

Fig. 2. SEM image (a) and its amplified picture (b), N_2-sorption isotherms (c) and pore size distribution (d) of the intermediate product MnO_2.

mesoporous material, meaning the nanoplates should be mesoporous. Such a meso-porosity can not only increase the contact area with the LiOH solution, but also enhance the combination of MnO_2 and CNT in the subsequent hydrothermal reaction step. Also, the BET surface area of the MnO_2 powder can be calculated as high as 27.1 $m^2\ g^{-1}$.

The SEM micrographs of the LMO/CNT and the annealed samples are presented in Fig. 3. Obviously, the carbon nanotubes are uniformly distributed in the LMO/CNT composite samples (Fig. 3a–c). The synthesized LMO particles keep a narrow particle size distribution at around 800 nm, while each carbon nanotube is connected with at least several LMO nanoparticles. In the samples S3 and S2 (Fig. 3a and b), the content of the CNT in the composites is not sufficient to connect all the LMO particles, so that the LMO particles are partly packed together without any CNT connection. For the sample S1 (Fig. 3c), the content of the CNT is sufficient to completely connect all the LMO particles and form a homogeneous dispersion network. From the amplified picture of the LMO particles (Fig. 3d), a small portion of LMO exhibits a shape of octahedron and co-exists with dominantly spherical LMO particles. The presence of LMO octahedrons suggests the high crystallinity of the composites. The spherical LMO particles are composed of about 100 nm-sized primary particles, which correspond to the nanoplate-assembled MnO_2 precursor. After the 450 °C annealing, there is no change in the morphology of LMO in S1 but most of the CNT have decomposed, so that the length of the CNT becomes shorter and there is very a small amount of CNT residue (Fig. 3e). When the annealing temperature is 700 °C (Fig. 3f), the CNT in the composite has been completely burnt out and no CNT residue can be detected by the SEM analysis.

The role of the CNT in the hydrothermal process is also studied. Without adding any CNT during the hydrothermal process, pure LMO phase cannot be obtained. Fig. S1a illustrates that part of the MnO_2 precursor cannot participate in the reaction with LiOH. After the annealing in air at 700 °C for 4 h, the MnO_2 has been converted into Mn_3O_4. Through adding 5 wt% CNT in the hydrothermal process, a LMO spinel phase combined with CNT can be obtained (Fig. S1a). The CNT component has been burned out and pure LMO phase has been remained after the annealing. Thus the CNT can act as a reducing agent that helps to convert MnO_2 completely into LMO with the presence of LiOH during the hydrothermal process. The SEM images in Fig. S2 can also confirm this point. Fig. S2a shows that part of the particles remains the burr-like spheres of the MnO_2 precursor, meaning MnO_2 is difficult to be converted into LMO without the CNT acting as a reducing agent. However, when 5 wt% CNT was added, the burr-like MnO_2 spheres have been converted into LMO spheres with the similar particle size (Fig. S2b). In addition, CNT can complex with LMO to form a LMO/CNT composite so as to improve the electronic conductivity of the electrode material.

Based on above structural analyses, we can draw a schematic illustration of the hydrothermal step (Scheme 1). The porous surface of MnO_2 offers a large contact area with CNT. Simultaneously, the acid-treated CNT has many −COOH and −OH on the surface so that a homogeneous starting mixture of MnO_2 nanoparticles with a well-dispersed CNT is obtained in the LiOH solution (Scheme 1a). After the hydrothermal treatment, a LMO/CNT composite is synthesized (Scheme 1c). The majority of the LMO is spherical particles while a minority of the LMO particles is octahedrons. Similar morphology was also reported by von Bulow et al. [26]. After the LMO/CNT composite has been annealed in air at a high temperature of 450 or 700 °C, the CNT hardly remains in the system (Scheme 1d).

To determine the content of CNT in the LMO/CNT composites, TG measurements were conducted in the temperature range from 20 to 750 °C in air atmosphere (Fig. 4 and Fig. 5). The results are listed

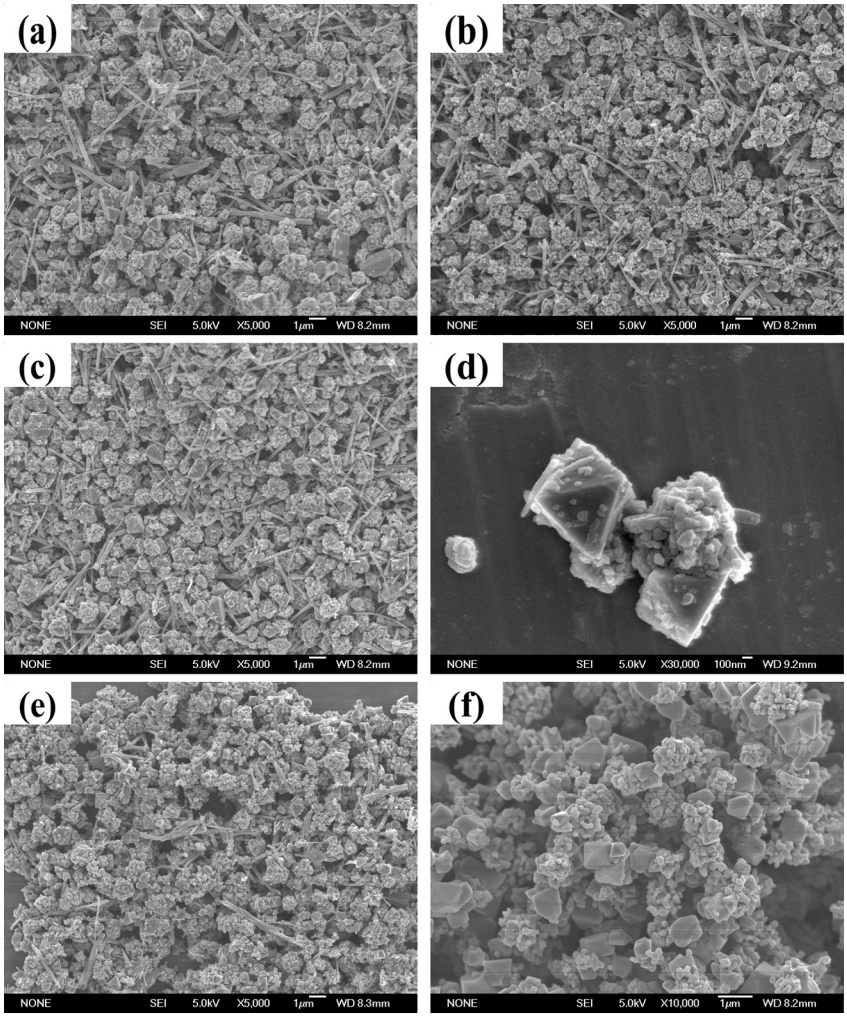

Fig. 3. SEM images of the hydrothermal products: S3 (a), S2 (b), S1 (c, d), S4 (e) and S5 (f) which were obtained by annealing S1 at 450 °C and 700 °C for 4 h in air.

in Table 1. For the composites S1–S3, the measured values of CNT content are about 2–4% less than those predicted from the starting compositions of MnO_2 and CNT. The differences may be caused by the material loss in the final centrifuging step. For the 450°C-annealed sample S4, there is still 2.74 wt% CNT residue, suggesting that CNT is not completely oxidized into CO_2 at 450 °C in air. In contrast, for the 700 °C heat-treated sample S5, no CNT residue is left.

The electrochemical properties of the synthesized LMO/CNT composites are shown in Fig. 6. All of the Li/(LMO/CNT) half-cells were cycled at 0.5C (1C = 120 mA g^{-1}) to activate the cathode materials. Fig. 6a reveals that the rate capability of the LMO/CNT is

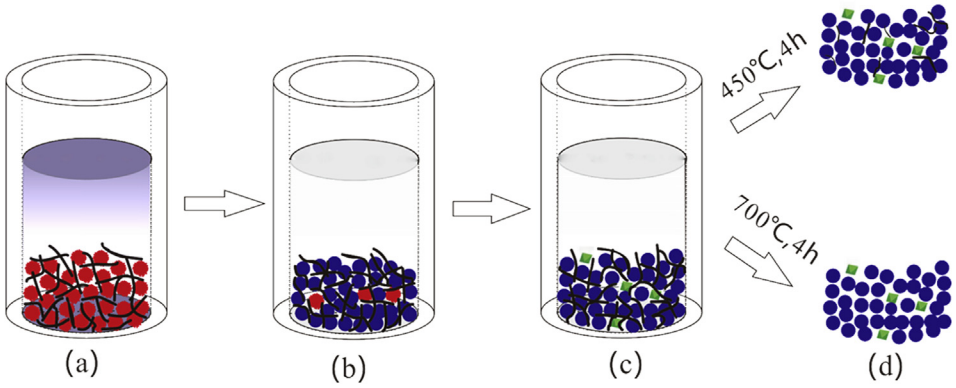

Scheme 1. Schematic illustration of the hydrothermal procedure: a) MnO_2 nanoparticles with well-dispersed CNT; b) intermediate product during the hydrothermal process; c) final product LMO/CNT after the hydrothermal step; d) annealing of the LMO/CNT at different temperatures.

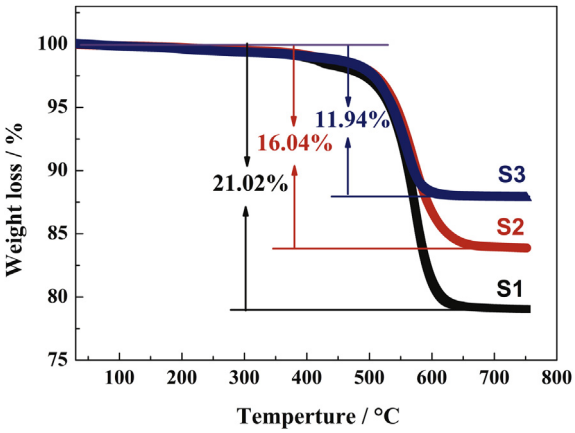

Fig. 4. TG curves of three LMO/CNT samples (S1–S3).

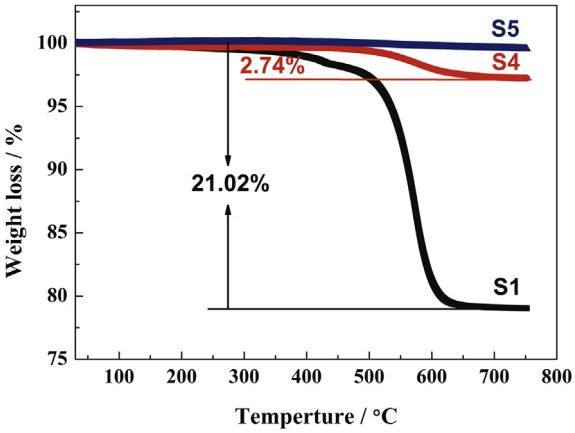

Fig. 5. TG curves of the pristine (S1) and its annealed LMO/CNT samples (S4, S5).

improved obviously with increasing the CNT content. The composite sample S1 exhibits a high reversible specific capacity of 125 mAh g^{-1} at 1C. Even at the charge–discharge current of 10C and 20C, the discharge capacity retention is 81.6% and 72% (corresponding to 102 and 90 mAh g^{-1}), respectively. For S2 and S3 with less CNT contents, the discharge capacity retention at 20C is 37.2% and 28.4% (corresponding to 43.7 and 30.8 mAh g^{-1}), respectively.

In order to compare our LMO/CNT samples with others, four papers on hydrothermal LMO/CNT composites are found [24–27]. Table 2 lists the comparison of their electrochemical properties with different contents of conducting additives. It is clearly seen that the electrochemical properties of our samples are better than those of ref. 25 and ref. 27 and slightly worse than those of ref. 24.

Table 1
CNT contents in the LMO/CNT samples measured by TG/DTA.

Sample	Heat treatment condition	CNT/(CNT + MnO_2) wt%	CNT/(CNT + LMO)	
			Predicted value	Measured value
S1	–	25%	24.18%	21.02%
S2	–	20%	19.38%	16.04%
S3	–	15%	14.51%	11.94%
S4	450 °C, 4 h	25%	–	2.74%
S5	700 °C, 4 h	25%	–	0.00%

Also, the capacity values reported in ref. 26 look somewhat higher than ours. However, the charge–discharge mode used in their measurement is different from ours in that they always keep the charge rate at 0.5C while we use charge@*n*C/discharge@*n*C ($n = 1, 2, 5, 10, 20$) mode, which would result in a lower capacity values at high rates. Therefore, the electrochemical properties of our composites are rather good.

To highlight the excellent high power capability of the hydrothermally synthesized composite, we annealed S1 at the temperatures of 450 °C or 700 °C in air to decompose partially or completely the CNT to obtain samples S4 and S5. As there are still 2.74 wt% and 0 wt% CNT in S4 and S5, we added different amount of CNT to ensure the samples to contain the same CNT content (21.02 wt%) as in S1 for electrochemical tests (Fig. 6). As shown in Fig. 6b, the specific capacity values of S1, S4 and S5 are similar at a low rate of 1C, but S1 has substantially higher capacity at high rates than S4 and S5. The reason is that CNT is dispersed more homogeneously in S1 by hydrothermal interaction than in S4 and S5 electrodes in which CNT is added mostly by simple mechanical mixing. Also, S4 is found to have the worst rate performance among the three electrodes. It appears that the annealing of S1 at 450 °C has an adverse effect on the electrochemical properties. The reason is likely that the electronic conductivity of the residual CNT (2.74 wt%) in S4 is very poor because of the oxidation of the CNT surface. The results of EIS measurement (Fig. 7) are consistent with the sequence of rate performances of S1, S4 and S5. It can be seen that all three cells have a similar ohmic resistance ($R_s \approx 4\ \Omega$), but the charge transfer resistance (R_{ct}) of S4 is the biggest ($R_{ct} \approx 132.1\ \Omega$) while it is only 75.8 Ω for S1. That means the LMO/CNT composite directly synthesized by the hydrothermal process can enhance the Li^+ transportation, leading to much improved high rate capability.

Fig. 6c shows the charge–discharge curves of S1 at different rates. The voltage profiles are typical for spinel-type $LiMn_2O_4$ with two obvious plateaus during the charge–discharge process even when the current increases from 1C to 5C [12]. Fig. 6d reveals the cycle performance of S1 at 10C with the first-cycle discharge capacity of 112 mAh g^{-1}. After 550 cycles, the discharge capacity still remains 83% (93 mAh g^{-1}). Fig. 8 shows the cyclic voltammograms (CV) of S1 electrode between 3.0 and 4.5 V vs. Li/Li^+ at a scan rate of 0.1 mV s^{-1}. The first cycle is shown with the black curve and the redox peaks are not sharp. In the following three cycles, two couples of the separate redox peaks are very sharp and unchanged. The voltage gap is also very small between the corresponding redox peaks due to a low resistance.

The excellent high power capability of the composites can be attributed to the following reasons. Firstly, we use a low temperature method to synthesize LMO that maintains the sub-micron spherical morphology of the intermediate product MnO_2. The fairly high BET surface area (16.3 $m^2\ g^{-1}$) can keep a large contact area with the electrolyte and facilitate fast Li-ion transport. Secondly and most importantly, an appropriate content of CNT in the composites can be well combined with the LMO nanoparticles to form a homogeneous dispersion network that can significantly increase the electronic conductivity of the composite.

4. Conclusions

The $LiMn_2O_4$/CNT (LMO/CNT) composites are successfully synthesized using a nanoplate-assembled MnO_2 as the Mn precursor through a two-step hydrothermal process. In the composites, the LMO component has a uniform submicron particle size while the CNT component is dispersed homogeneously. The composite with 21.02 wt% CNT shows the optimal electrochemical performance with discharge capacities of 125, 102 and 90 mAh g^{-1}

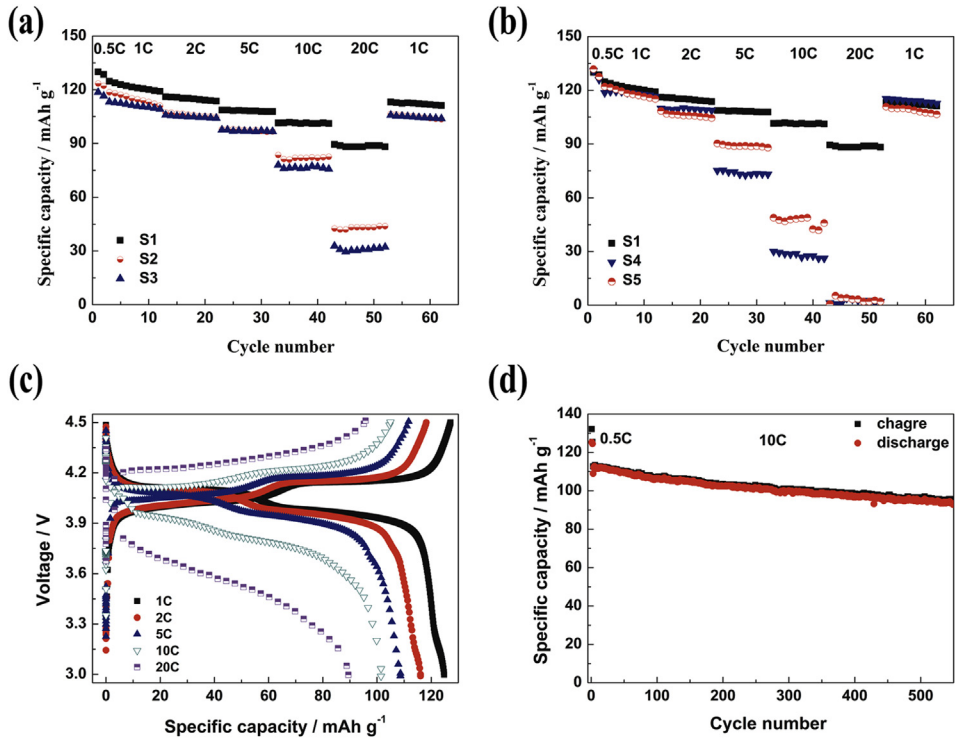

Fig. 6. Electrochemical performance of the LMO/CNT composites: rate capability (a, b), charge–discharge curves of S1 at different C rates (c) and its long cycling performance at 10C (d).

Table 2
Comparison of the electrochemical performance of the LMO/CNT samples between literature results and this work.

Ref. no.	Conducting additives (wt%)		Discharge capacity (mAh g^{-1})				
	CNT	Carbon black	1C	2C	5C	10C	20C
24	20	0	124	123	120	106	–
25	10.5	20	–	–	102	93	–
26 (0.5C charge)	10	5	123	122	121	116	94
27	35	15	118	117	100	83	–
Our work	21	0	124	117	109	102	90

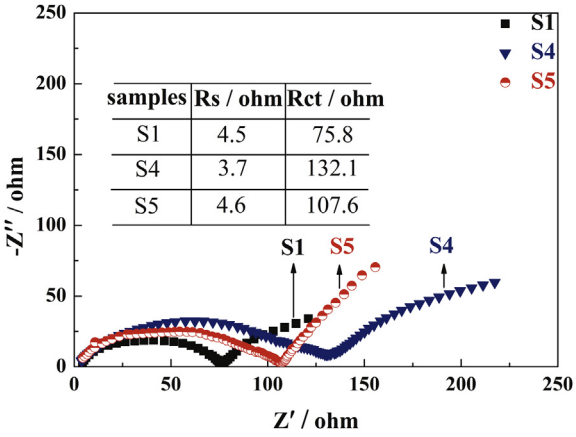

Fig. 7. Electrochemical impedance spectra of three half cells Li/S1, Li/S4 and Li/S5 after the 1st cycle at 0.5C rate and being charged to about 50% SOC. The open circuit voltage of the cells was 4.0 V.

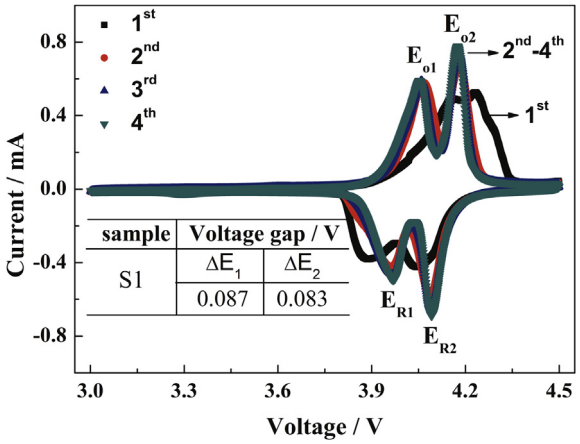

Fig. 8. Cyclic voltammograms (CV) of S1 electrode between 3.0 and 4.5 V vs. Li/Li^+ at a scan rate of 0.1 mV s^{-1}.

at 1C, 10C and 20C, respectively. Such a superior performance indicates that the LMO/CNT composite has a great potential as a cathode material of lithium ion batteries for in high-power applications.

Acknowledgments

This study was supported by National Natural Science Foundation of China (grant no. 20971117, 10979049 and J1030412) and Education Department of Anhui Province (grant no. KJ2009A142). We are also grateful to Elementec Ltd in Suzhou.

Appendix A. Supplementary data

Supplementary data related to this article can be found at http://dx.doi.org/10.1016/j.jpowsour.2014.06.085.

References

[1] A.S. Arico, P. Bruce, B. Scrosati, Nat. Mater. 1 (2005) 366–377.
[2] Y.G. Guo, J.S. Hu, L.J. Wan, Adv. Mater. 20 (2008) 2878–2887.
[3] C. Liu, F. Li, L.P. Ma, H.M. Cheng, Adv. Energy Mater. 22 (2010) E28–E62.
[4] J.B. Goodenough, Y. Kim, Chem. Mater. 22 (2010) 587–603.
[5] J.M. Tarascon, M. Armand, Nature 414 (2010) 359–367.
[6] J. Cho, Y.J. Kim, B. Park, Chem. Mater. 12 (2000) 3788–3791.
[7] K. Ozawa, Solid State Ionics 69 (1994) 212–221.
[8] Y.S. Jung, A.S. Cavanagh, A.C. Dillon, M.D. Groner, S.M. George, S.H. Lee, J. Electrochem. Soc. 157 (2010) A75–A81.
[9] S.Y. Chung, J.T. Bloking, Y.M. Chiang, Nat. Mater. 1 (2002) 123–128.
[10] L.X. Yuan, Z.H. Wang, W.X. Zhang, X.L. Hu, J.T. Chen, Y.H. Huang, J.B. Goodenough, Energy Environ. Sci. 4 (2011) 269–284.
[11] R.J. Gummow, A. Dekock, M.M. Thackeray, Solid State Ionics 69 (1994) 59–67.
[12] J.M. Tarascon, E. Wang, F.K. Shokoohi, W.R. Mckinnon, S. Colson, J. Electrochem. Soc. 138 (1991) 2859–2864.
[13] X.D. Xiang, Z. Fu, W.S. Li, J. Solid State Electrochem. 17 (2013) 1201–1206.
[14] H.W. Chan, J.G. Duh, S.R. Sheen, J. Power Sources 115 (2003) 110–118.
[15] F.Y. Cheng, H.B. Wang, Z.Q. Zhu, Y. Wang, T.R. Zhang, Z.L. Tao, J. Chen, Energy Environ. Sci. 4 (2011) 3668–3675.
[16] Y. Qiao, S.R. Li, Y. Yu, C.H. Chen, J. Mater. Chem. A 1 (2013) 860–867.
[17] Y.L. Ding, X.B. Zhao, J. Xie, G.S. Cao, T.J. Zhu, H.M. Yu, C.Y. Sun, J. Mater. Chem. 21 (2011) 9475–9479.
[18] J.Y. Luo, H.M. Xiong, Y.Y. Xia, J. Phys. Chem. C 112 (2008) 12051–12057.
[19] K.M. Shaju, P.G. Bruce, Chem. Mater. 20 (2008) 5557–5562.
[20] D. Song, H. Ikuta, T. Uchida, M. Wakihara, Solid State Ionics 117 (1999) 151–156.
[21] D. Capsoni, M. Bini, G. Chiodelli, V. Massarotti, P. Mustarelli, L. Linati, M.C. Mozzati, C.B. Azzoni, Solid State Commun. 126 (2003) 169–174.
[22] L.L. Xiong, Y.L. Xu, T. Tao, J.B. Goodenough, J. Power Sources 199 (2012) 214–219.
[23] A. Yamada, M. Tanaka, Mater. Res. Bull. 30 (1995) 715–721.
[24] H. Xia, K.R. Ragavendran, J.P. Xie, L. Lu, J. Power Sources 212 (2012) 28–34.
[25] M.X. Tang, A.B. Yuan, H.B. Zhao, J.Q. Xu, J. Power Sources 235 (2013) 5–13.
[26] J.F. von Bulow, H.L. Zhang, D.E. Morse, Adv. Energy Mater. 2 (2012) 309–315.
[27] Y.H. Ding, J.X. Li, Y. Zhao, L.H. Guan, Mater. Lett. 68 (2012) 197–200.